Molecular Weight Dependence of Phase Structures and Transitions of Mesogen-Jacketed Liquid Crystalline Polymers Based on 2-Vinylterephthalic Acids

Chun Ye,[†] Hai-Liang Zhang,[†] Yun Huang,[†] Er-Qiang Chen,*[,†] Yonglai Lu,[‡] Deyan Shen,[‡] Xin-Hua Wan,[†] Zhihao Shen,[§] Stephen Z. D. Cheng,[†,§] and Qi-Feng Zhou*[,†]

Department of Polymer Science and Engineering, College of Chemistry and Molecular Engineering, Peking University, Beijing 100871, China; State Key Laboratory of Polymer Physics and Chemistry, Center for Molecular Science, Institute of Chemistry, Chinese Academy of Science, Beijing 100080, China; and Maurice Morton Institute and Department of Polymer Science, The University of Akron, Akron, Ohio 44325-3909

Received April 26, 2004; Revised Manuscript Received June 30, 2004

ABSTRACT: The phase structures and transition behaviors of a series of mesogen-jacketed liquid crystalline (LC) polymers, poly{2,5-bis[(4-methoxyphenyl)oxycarbonyl]styrenes} (PMPCS), with different molecular weights (MW) and narrow MW distributions were studied using differential scanning calorimetry, polarized light microscopy, Fourier transform infrared spectroscopy, and one- and two-dimensional wide-angle X-ray diffraction experiments. The LC phase structures of this series of PMPCS samples were found to be strongly MW dependent. The PMPCS samples were amorphous when the MW is lower than a critical MW of approximately 1.0×10^4 g/mol (an apparent MW, M_n^a, measured by gel permeation chromatography calibrated with the polystyrene standards). For the PMPCS samples with MWs higher than this critical value, the amorphous samples cast from solution developed into a LC phase above the glass transition temperature upon the first heating. In between 1.0×10^4 g/mol $< M_n^a < 1.6 \times 10^4$ g/mol, a columnar nematic (Φ_N) phase was stabilized. Above the $M_n^a = 1.6 \times 10^4$ g/mol, a hexatic columnar nematic (Φ_{HN}) phase was observed. Within these two LC phases, the building blocks were cylindrical shaped, which was attributed to a cooperative assembly of the PMPCS backbone and its laterally attached mesogenic groups. The diameter of this cylindrical building block was in the vicinity of 1.6 nm as determined by WAXD experiments. All the LC phases were found to be stable up to the decomposition temperature of the PMPCS samples. The MW dependence of the LC phase diagram indicated that a critical aspect ratio (the ratio between the length and diameter of the cylinders) of the cylindrical building blocks must be required to stabilize these LC phases. On the basis of Flory's calculation, the critical aspect ratio should be 5.44, and this value corresponded to critical cylinder lengths of around 8−9 nm. Therefore, the lowest degree of polymerization which would stabilize the LC phases is ∼39−42 for this series of PMPCS samples.

Introduction

Phase structures and transitions of thermotropic liquid crystalline (LC) polymers have been one of the important topics to study in polymer chemistry and physics for the past several decades. Through designed synthetic strategies, the incorporation of mesogenic groups (rigid rods and disks) in LC polymers results in several molecular architectures that can lead to different mesomorphic structures and dynamic behaviors. The main-chain and side-chain LC polymers are the two most common categories based on the locations of the mesogenic groups in polymers.[1,2] In both of these two types of LC polymers, flexible spacers introduced between the mesogens in main-chain LC polymers or between backbones and mesogens in side-chain LC polymers can usually improve the mobility of the mesogenic groups and facilitate the formation of LC phase structures. Moreover, in the side-chain LC polymers with mesogenic groups either terminally or laterally attached to backbones, the insertion of spacers with reasonable lengths decouples the dynamics of the backbone and the mesogens.[3,4]

In the past several years, we have focused on the design and synthesis of side-chain LC polymers with the mesogens laterally attached to backbones via a short linkage or a single carbon−carbon bond. They have been called "mesogen-jacketed liquid crystalline polymers" (MJLCP).[5−15] Four series of MJLCPs, which were based on 2-vinylhydroquinone,[6−8] 2-vinyl-1,4-phenylenediamine,[8,9] 2-vinylterephthalic acid,[10−13] and 2-vinyl-*p*-terphenyl,[14,15] were synthesized and investigated. All of these polymers exhibit LC phase behaviors. However, the LC phase structures of these polymers are characteristically different from those of common terminally attached side-chain LC polymers. This is illustrated by the ease with which the MJLCP samples display banded textures after mechanical shearing in their LC states[16] and possess larger persistent lengths in solution.[17] It is conceivable that in these MJLCP samples the bulky mesogenic groups linked to every second carbon atom along the backbones without spacers or with very short linkages introduce significant steric hindrance of the mesogens and thereby enhance the stiffness of polymer backbones to form rodlike chains.[5,16−20] As a result, the backbones and mesogens in these MJLPC samples are strongly coupled in the formation of LC phases.

Different from those low-ordered LC phases, namely, nematic (N), smectic A (S_A), and C (S_C) phases com-

[†] Peking University.
[‡] Chinese Academy of Science.
[§] The University of Akron.
* To whom the correspondence should be addressed.

10.1021/ma049195b CCC: $27.50
Published on Web 08/25/2004

Table 1. Molecular Characteristics of the PMPCS Samples[a]

sample	P-1	P-2	P-3	P-4	P-5	P-6	P-7	P-8	P-9	P-10	P-11	P-12	P-13	P-14
M_n[a]	0.23	0.26	0.30	0.40	0.50	0.57	0.71	0.80	0.90	1.02	1.32	1.59	1.94	2.55
dw	1.07	1.08	1.09	1.12	1.12	1.13	1.13	1.15	1.10	1.14	1.18	1.15	1.19	1.20

[a] The apparent number-average molecular weight M_n[a]s [$\times 10^{-4}$ (g/mol)] were measured by GPC using a monodisperse PS as a calibration standard.

monly observed in laterally attached side-chain LC polymers,[4,21−27] the MJLCP samples may present columnar LC phases like those in LC polymers with disklike mesogens incorporated in the polymers. The polymers containing disklike mesogens exhibit low-ordered phases such as the discotic nematic (N_D), columnar nematic (Φ_N), and high-ordered two-dimensional hexagonal columnar (Φ_H) phases, etc.[28−38] Recently, the Φ_H and tilted Φ_H phases were also identified in a series of linear randomly copolymerized LC copolyethers without disklike mesogens,[39−41] vinyl polymers with sterically hindering, laterally attached, bulky side groups, which are close to the MJLCP,[42−45] and monodendron-jacketed polymers.[46−50] It has been found that some of the poly[di(alkyl) vinylterephthalates] (PDAVT)[42−45] synthesized based on 2-vinylterephthalic acids exhibit the Φ_H phase[43,45] even though neither the backbones nor the side groups exhibit LC behavior. The backbone may adopt a somewhat extended (likely, helical) conformation surrounded by the bulky side groups to form the cylinders that are the building blocks from which the Φ_H phase develops.

In this study, a series of poly{2,5-bis[(4-methoxyphenyl)oxycarbonyl]styrenes} (PMPCS) with different MWs were synthesized via the atomic transfer radical polymerization (ATRP). The chemical structure of the PMPCS is as follows:

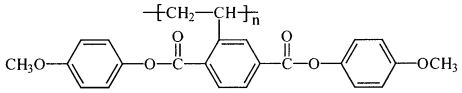

The controlled MWs ranged from 10^3 to 10^4 g/mol with narrow MW distributions. The resultant series of the PMPCSs is therefore a model system to clarify the effect of the MW on the LC phase structures and phase transitions of MJLCPs. The PMPCS studied exhibits columnar LC phases when the apparent MW measured by gel permeation chromatography (GPC) based on polystyrene (PS) calibration standards exceeds approximately 1.0×10^4 g/mol. We believe that the cooperative accommodation of the laterally attached mesogenic groups surrounding the extended PMPCS backbones may construct the cylindrical building blocks from which the polymers self-assemble into the columnar phases.

Experimental Section

Materials and Samples. The series of PMPCS samples with different MWs was synthesized using ATRP that was catalyzed with CuBr/sparteine (Sp) and initiated by 1-bromoethylbenzene (BEB) in methoxybenzene. The detailed synthetic procedure and the chemical characterization of the monomer and polymers are reported eleswhere.[10,11,13,51] The apparent number-average molecular weight (M_n[a]) and polydispersity (*dw*) of the PMPCS samples studied were measured by GPC (Waters 150C) equipped with three Waters Styragel columns (10^2, 10^3, and 10^4 nm), which was calibrated with PS standard samples. The MW characterization of the PMPCS samples is listed in Table 1. The decomposition temperature (T_d) of the samples with a heating at a rate of 10 °C/min was ∼350 °C in a dry nitrogen atmosphere.

For heat capacity (C_p) measurements in differential scanning calorimetry (DSC), the samples were cast from THF solution and dried at 50 °C under a vacuum. The samples were then kept under vacuum for several days. The dried samples had a thickness of nearly 0.2 mm. A typical mass of ∼10 mg was encapsulated in a sealed aluminum pan with the pan weight identically matched to the reference pan for the C_p measurements. The samples were first heated to 250 °C and then cooled to −10 °C at 10 °C/min. This was followed by a second heating scan.

For one-dimensional (1D) wide-angle X-ray diffraction (WAXD) powder experiments, the polymer films were identical to those prepared in the DSC experiments. For two-dimensional (2D) WAXD experiments, the oriented samples were prepared by mechanically shearing the films in the LC phases at a temperature between 180 and 220 °C.

In both the polarized light microscopy (PLM) and Fourier transform infrared spectroscopy (FT-IR) experiments, the film samples were prepared by THF solution directly casting on clean cover glass or KBr pellets, respectively. The oriented samples for PLM and FT-IR were also obtained by mechanical shearing in the LC phases. For the density measurement, the PMPCS samples cast from THF solutions were annealed at 200 °C for 2 h and slowly cooled to room temperature.

Instrument and Experiments. The C_p measurements were conducted with a Perkin-Elmer Pyris I DSC with a mechanical refrigerator. The temperatures and heat flows were calibrated using standard materials such as benzoic acid and indium, and the C_p was calibrated using single-crystal sapphire. Each C_p measurement included three runs: the empty pans for baseline determination, the sapphire for the C_p calibration, and the sample run.[52] The C_p is determined after the steady state was reached at a heating rate of 10 °C/min.

1D WAXD powder experiments were performed on a Philips X'Pert Pro diffractometer with a 3 kW ceramic tube as the X-ray source (Cu Kα) and an X'celerator detector. The sample stage was set horizontally. The reflection peak positions were calibrated with silicon powder ($2\theta > 15°$) and silver behenate ($2\theta < 10°$). Background scattering was recorded and subtracted from the sample patterns. A temperature control unit (Paar Physica TCU 100) in conjunction with the diffractometer was utilized to study the structure evolutions as a function of temperature. The heating and cooling rates in the WAXD experiments were 1.5 °C/min.

2D WAXD fiber patterns were obtained using a Bruker D8Discover diffractometer with GADDS as a 2D detector. Again, calibration was conducted using silicon powder and silver behenate. Samples were mounted on the sample stage, and the point-focused X-ray beam was aligned both perpendicular and parallel to the mechanical shearing direction. The 2D diffraction patterns were recorded in a transmission mode at both room temperature and 180 °C.

A Leica DML PLM with a Mettler hot stage (FP-90) was used for the LC texture observations. A FT-IR (Magna-IR 750) was employed to measure IR absorption spectrum of the samples. To characterize the chemical group orientation in the oriented samples, polarized FT-IR measurements were also performed. The density measurements of the PMPCS samples were conducted using a flotation technique. An aqueous solution of KI at room temperature was used. The sample equilibrated with the KI solution after matching the buoyancy of the sample and the surrounding liquid, and thus, the sample was floated freely for an extended period of time. A pycnometer was then filled with the KI solution to be weighed.

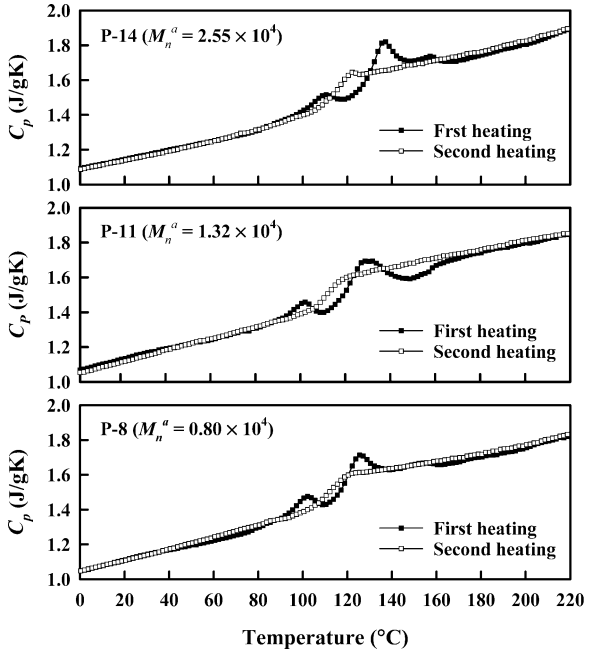

Figure 1. Set of DSC thermal diagrams during the first and second heating of the PMPCS samples with the $M_n{}^a = 2.55 \times 10^4$ (P-14), 1.32×10^4 (P-11), and 0.80×10^4 (P-8) at a rate of 10 °C/min, respectively. The plots show heat capacity change with respect to temperature. The second heating was after the samples were heated to 250 °C and then cooled to −10 °C at the rate of 10 °C/min.

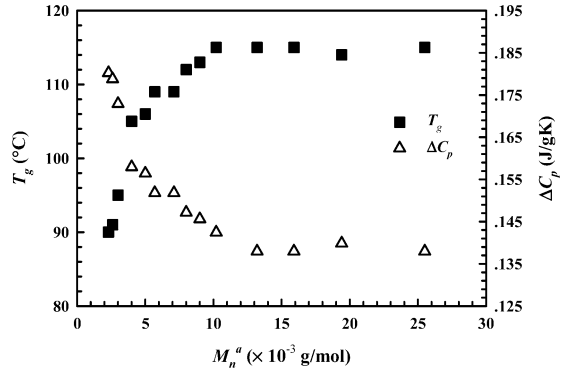

Figure 2. T_g values of PMPCS samples measured during the second heating as a function of different MWs. The ΔC_p values at the glass transition as a function of MW are also included.

Results and Discussion

Phase Behaviors of PMPCS Samples during Heating and Cooling. The solution-cast PMPCS samples with different $M_n{}^a$ values exhibited complex thermal behaviors shown in the first DSC heating thermal diagrams (see Figure 1). We will focus on the second heating DSC thermal diagrams since the previous thermal histories of these samples were erased. Figure 1 shows an example set of the DSC second heating diagrams of three PMPCS samples (P-14, P-11, and P-8) with the $M_n{}^a$ values of 2.55×10^4, 1.32×10^4, and 0.80×10^4 g/mol, respectively (for the purpose of these selections, see below). On the basis of the C_p results, a glass transition process can be observed in all these samples. Figure 2 shows that the glass transition temperatures (T_g) of the PMPCS samples, defined by a temperature at which a 50% devitrification takes place, increases with increasing the $M_n{}^a$, and reaches a plateau of 116 °C when the $M_n{}^a$ exceeds approximately 1.0×10^4 g/mol. Furthermore, since the C_p−temperature dependences in the glass and liquid states are different, we find that the ΔC_p is also $M_n{}^a$ dependent as shown in Figure 2. Only when the $M_n{}^a$ exceeds 1.0×10^4 g/mol does the ΔC_p reach a constant of 0.138 J/(g K).

It is noted that no latent heat (i.e., no first-order transition) can be detected in the DSC thermal diagrams for all these PMPCS samples during the first cooling and subsequent heating scans between −10 and 250 °C. To examine whether the ordered structures developed in these polymers, we utilized 1D WAXD experiments to investigate the as-cast PMPCS samples during the first heating. It is found that during the first heating the phase structural development in the as-cast PMPCS samples is strongly MW-dependent. Three $M_n{}^a$ regimes have been identified on the basis of 1D WAXD experimental results: the high MW regime with the $M_n{}^a$ exceeding 1.6×10^4 g/mol, the low MW regime with the $M_n{}^a$ below 1.0×10^4 g/mol, and the intermediate MW regime with the $M_n{}^a$ between these two $M_n{}^a$ values. We will thus use P-14 ($M_n{}^a = 2.55 \times 10^4$ g/mol), P-11 ($M_n{}^a = 1.32 \times 10^4$ g/mol), and P-8 ($M_n{}^a = 0.80 \times 10^4$ g/mol) (see Table 1) as representatives for these three MW regimes.

Parts a and b of Figure 3 illustrate the two sets of 1D WAXD patterns of the as-cast P-14 sample obtained during the first heating in both the low 2θ (between 2° and 10°) and high 2θ (between 10° and 30°) angle regions, respectively. In Figure 3a, the low angle scattering halo is observed when the temperature is below 140 °C. Upon heating, this scattering halo undergoes a dramatic change starting at 140 °C; i.e., the halo increases its intensity and suddenly shifts to higher 2θ angles. At 160 °C, the scattering halo becomes asymmetric and can be deconvoluted into one broad halo and one narrow reflection peak with centers at $2\theta = 5.6°$ (d spacing of 1.58 nm) and 5.8° (d spacing of 1.51 nm), respectively (the dashed curves in Figure 3a). This deconvolution was carried out utilizing two Gaussian functions to precisely identify the center d spacings of the halo and reflection peak. (This peak deconvolution method will also used in the 1D WAXD data of other PMPCS samples in this study.) When temperature reaches 180 °C, the two d spacing values corresponding to the halo and peak are dropped to be 1.57 and 1.48 nm, respectively. Further heating the P-14 sample leads to a substantial enhancement of the reflection peak intensity, and the peak position continuously and slightly shifts to lower 2θ angles. The completely evolved reflection peak at 240 °C shows a d spacing of 1.50 nm.

In Figure 3b, the high angle scattering halo ($2\theta \sim 20°$) retains the same shape upon heating. With increased temperatures, however, the center of this halo at $2\theta = 20.5°$ (d spacing of 0.43 nm) slightly shifts to lower 2θ angles in the beginning, followed by a sudden jump to $2\theta = 19.5°$ (d spacing of 0.45 nm) between 140 and 180 °C. Above 180 °C, a slight and continuous shift of this center position to lower 2θ angles caused by the thermal expansion in the liquid of the sample is observed. This sudden shift corresponds to the formation of the ordered structure observed in Figure 3a on the nanometer length scale. However, no long-range order developed in the sub-nanometer length scale during the heating.

After the first heating to 240 °C, a cooling WAXD experiment of the P-14 was carried out, as shown in parts c and d of Figure 3 for both the low and high 2θ angle regions, respectively. In the low angle region (Figure 3c), the evolved reflection peak at $2\theta \sim 6.0°$

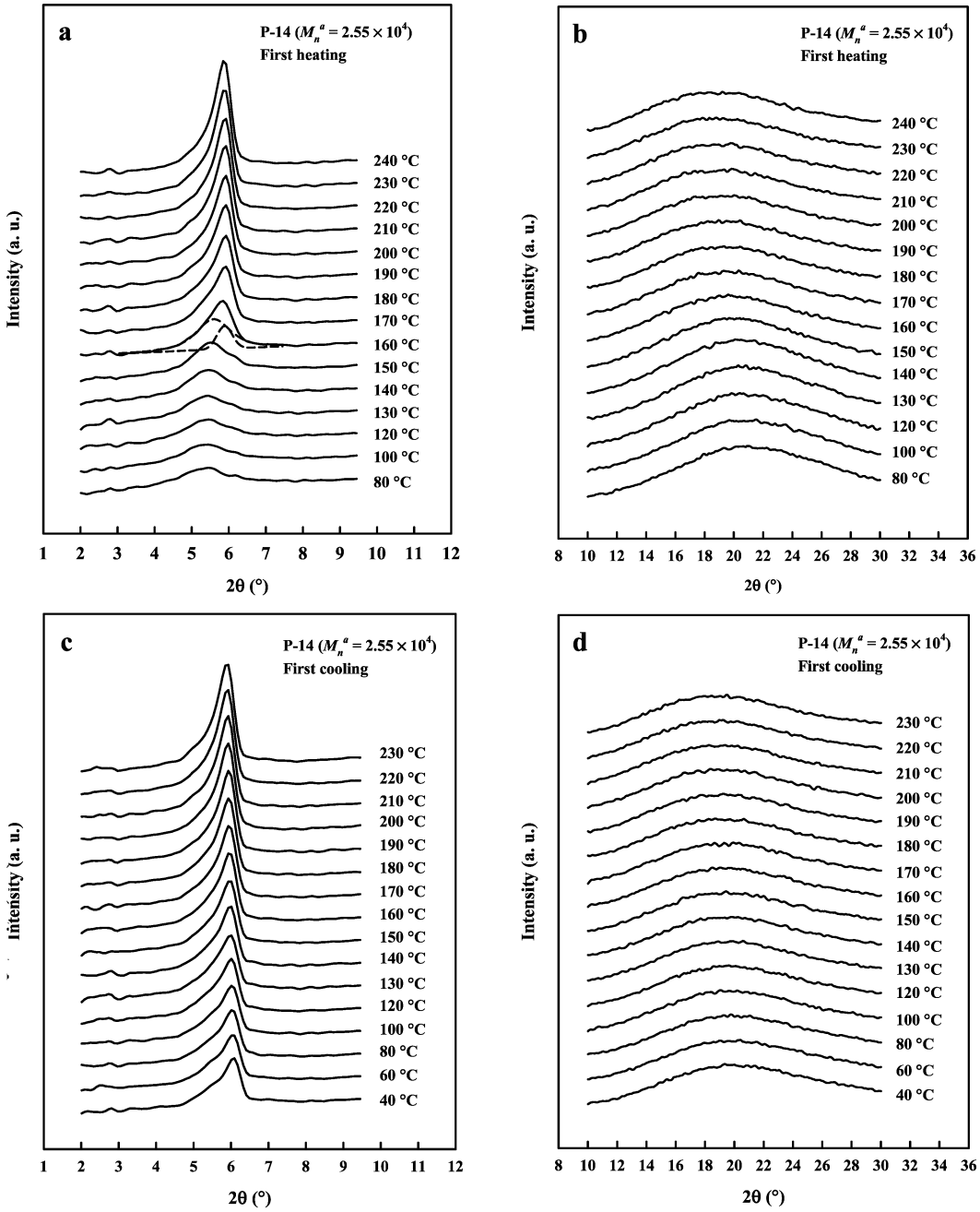

Figure 3. Sets of WAXD powder patterns in the low 2θ angle region (a) and in the high 2θ angle region (b) of P-14 obtained during the first heating of the as-cast film. The corresponding first cooling WAXD powder patterns in both low and high 2θ angle regions are shown in (c) and (d). To show the development of the reflection peak in the low 2θ angle region, the deconvolution of the reflection peak from the scattering halo is shown by the dashed curves at 160 °C in (a).

stays permanently. Moreover, the reflection peak intensity decreases with decreasing temperatures. For example, the intensity at 40 °C is only nearly half of the one at 230 °C. This indicates that the periodic electron density contrast generating this reflection reduces with decreasing temperature. On the other hand, the cooling 1D WAXD patterns in the high 2θ angle region in Figure 3d do not exhibit the sudden shift of the center *d* spacing of the halo as observed in the first heating of the as-cast sample shown in Figure 3b.

Parts a and b of Figure 4 quantitatively summarize the *d* spacing changes with temperatures for the P-14 in the low and high 2θ angle regions, respectively, during the fist heating and subsequent cooling. In Figure 4a, the slope of the cooling lines represents the coefficients of thermal expansion (CTE) of the structures studied, and the value is approximately 2.0×10^{-4} nm/°C. Moreover, the CTE value obtained from the cooling experiments does not significantly change at the T_g, indicating that the nano-ordered structure is not responsible for the glass transition process. Subsequent heating and cooling experiments do not further change CTE value and the temperature dependence of the *d* spacing observed in the first cooling. On the other hand, the cooling data in the high 2θ angle region in Figure 4b only show a slope change between 140 and 120 °C, indicating that a vitrification process occurs on the structure of this length scale. For the temperature regions below and above 130 °C, the two CTE values are 6.1×10^{-5} and 2.0×10^{-4} nm/°C, respectively.

In the first heating of the as-cast P-11 samples, the low 2θ angle 1D WAXD patterns are shown in Figure

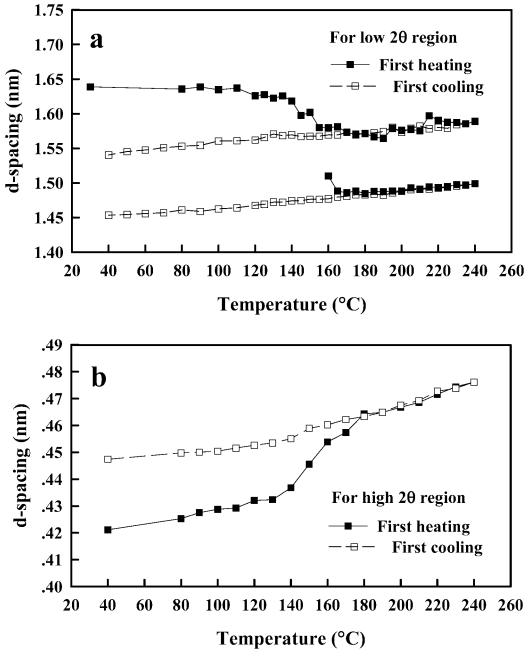

Figure 4. *d*-spacing data as functions of temperature measured during the first heating and subsequent cooling in the low 2θ angle WAXD powder patterns (a) and in the high 2θ-angle region of P-14 (b).

5a. The center of the scattering halo exhibits a large shift toward a higher 2θ angle between 120 and 140 °C. At 190 °C, a shoulder appears on the higher angle side of this halo (the dashed curves in Figure 5a are the deconvoluted halo and peak) and develops into a reflection peak with a further increase in temperature (2θ = 5.5° with a *d* spacing of 1.61 nm at 240 °C). Compared with the reflection peak of the P-14 shown in Figure 3a, this peak is broader with a medium intensity. During the subsequent cooling, the reflection peak and scattering halo are retained down to room temperature. Both of the intensities of the reflection peak and the scattering halo decrease with decreasing temperature. On the other hand, the scattering halos of P-11 at 2$\theta \sim$ 20° exhibit similar behaviors as that of P-14. Figure 5b illustrate quantitatively the *d* spacings corresponding to the halo and peak in the low 2θ angle region as functions of temperature upon the first heating and subsequent cooling. The CET measured from the cooling data is found to be similar to the case of P-14.

In the as-cast P-8 sample, the 1D WAXD patterns in Figure 6a exhibit that the scattering halo increases in intensity with increasing temperature but remains as a broad scattering for the entire temperature region. Upon the first heating, the center of the scattering halo at a *d* spacing of ~1.73 nm at room temperature gradually shifts to high 2θ angles when temperature is below 130 °C. This observation is opposite to the commonly observed thermal expansion during heating, and the gradual decrease of the *d* spacing is also different from those observed in P-14 and P-11, where the sudden decreases of the *d* spacings are observed (Figures 3a and 5a). After heating to above 130 °C, the molecules have enough mobility to achieve the dense equilibrium packing in the isotropic melt, and the scattering halo starts to shift to low 2θ angles. During the subsequent cooling, the center *d* spacing of the halo continuously decreases, indicating that this dense structure is retained. The CTE value is again similar to both the cases of P-14 and P-11. Figure 6b represents the

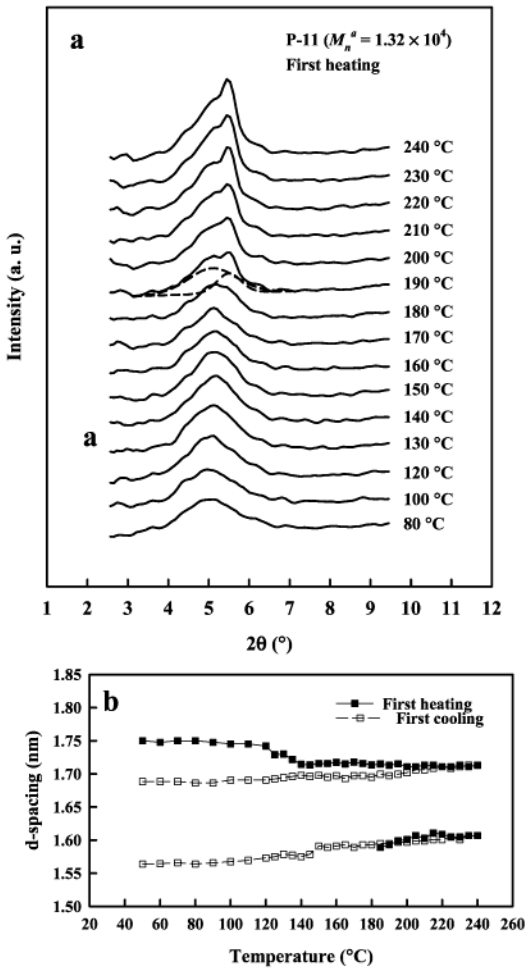

Figure 5. (a) Set of low 2θ angle WAXD powder patterns of P-11 obtained during the first heating of the as-cast films. The dashed curves at 190 °C in (a) represent the deconvolution results between the scattering halo and the reflection peak. (b) *d* spacing data as functions of temperature measured during the first heating and cooling sequence in the low 2θ angle WAXD powder patterns for P-11.

quantitative changes of the scattering halo *d* spacing in the low 2θ angle region with temperatures during the first heating and subsequent cooling. Note that these is no reflection peak can be observed in this sample.

On the basis of these 1D WAXD results, it can be concluded that the as-cast samples are amorphous on two different length scales of the structures. For the PMPCS samples with the $M_n{}^a > 1.0 \times 10^4$ g/mol, the ordered structures on the nanometer scale develop during the first heating above their T_g values. After this process, the ordered structures are permanently retained in the subsequent cooling and heating scans. However, the 1D WAXD patterns lack dimensionality, and 2D WAXD fiber patterns are necessary to identify the phase structures.

Phase Identifications of the PMPCS Samples. Parts a and b of Figure 7 are two 2D WAXD patterns at room temperature of the oriented P-14 and P-11 samples, respectively, with the X-ray incident beam perpendicular to the fiber axis. In these two figures, the fiber axis is parallel to the meridian direction. A pair of strong diffraction arcs can be seen on the equators at 2θ = 6.1° (*d* spacing of 1.45 nm) and 5.7° (*d* spacing of 1.56 nm) for P-14 and P-11, respectively, indicating that the ordered structures have developed along the

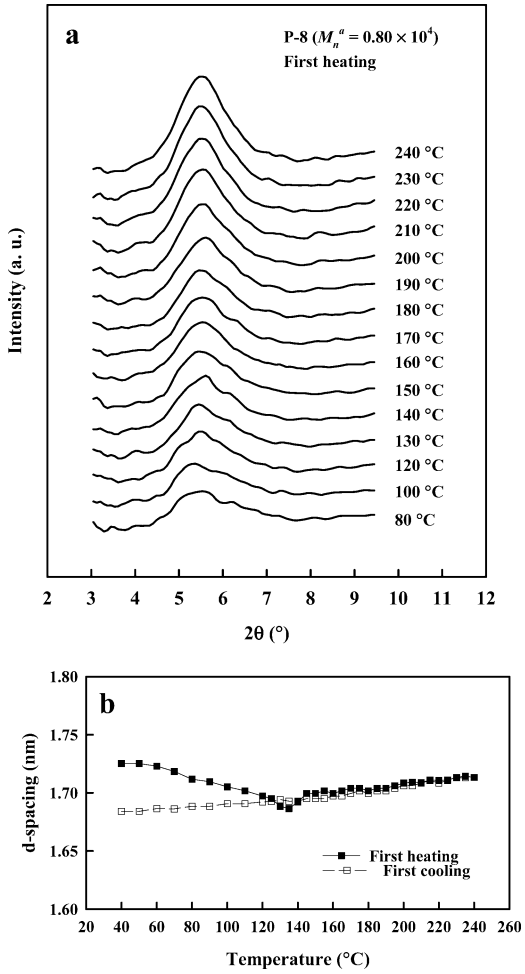

Figure 6. (a) Set of low 2θ angle WAXD powder patterns of P-8 obtained during the first heating of the as-cast films. (b) *d* spacing data as functions of temperature measured during the first heating and cooling sequence in the low 2θ angle WAXD powder patterns for P-8.

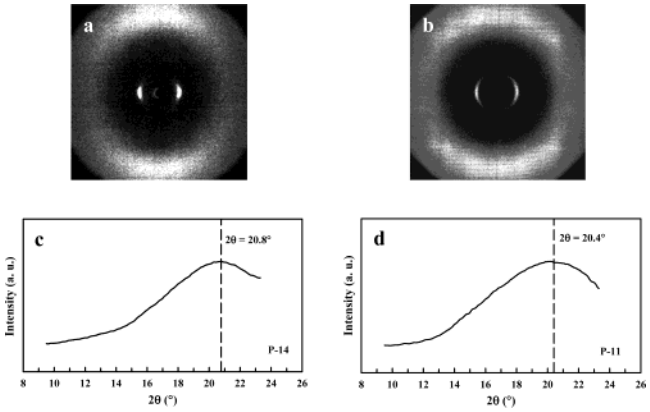

Figure 7. 2D WAXD fiber patters of P-14 (a) and P-11 (b) obtained at room temperature. The X-ray incident beam is perpendicular to the fiber axis (the meridian direction). The intensity profiles (c) and (d) are along the meridian obtained from (a) and (b), respectively.

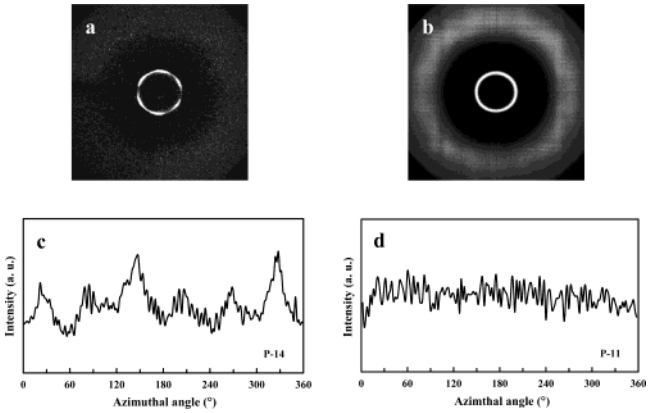

Figure 8. 2D WAXD fiber patters of P-14 (a) and P-11 (b) detected at room temperature. The X-ray incident beam is parallel to the fiber axis. The azimuthal scanning data of the low 2θ angle diffraction of P-14 and P-11 are shown in (c) and (d), respectively.

direction perpendicular to the fiber axis on the nanometer scale. On the other hand, scattering halos in the high 2θ angle region are more or less concentrated on the meridians with rather broad azimuthal distributions. This reveals that only the short-range orders exist along the fiber direction. Parts c and d of Figure 7 are the intensity profiles along the meridian, wherein the amorphous scattering maxima are located at $2\theta = 20.8°$ and 20.4° (*d* spacing of 0.426 and 0.435 nm), respectively, for the P-14 and P-11 samples.

For the strong diffraction pairs in the low 2θ angle region on the equators in Figure 7a,b, we did not find the higher order diffractions even when the 2D WAXD experiments were performed on the annealed samples at a high temperature of 180 °C (where the scattering intensities are much stronger than that at room temperature) with prolonged exposure times. To determine the symmetry of these ordered phases, the X-ray incident beam was aligned parallel to the fiber axis, and the diffraction patterns of the P-14 and P-11 samples are shown in Figure 8a,b. In the case of P-14, six diffraction arcs are located at $2\theta = 6.1°$ (*d* spacing of 1.45 nm). The corresponding azimuthal intensity profile shown in Figure 8c exhibits six maxima with an angle of 60° between the two adjacent diffraction maxima, although the intensities are not exactly identical (this may be caused by imperfection in the sample orientation during the experiment). This indicates a hexagonal lateral packing of the cylinders with each cylinder having an average diameter of 1.67 nm. However, this hexagonal lateral packing lacks long-range order perpendicular to the fiber axis, since the higher order diffractions are missing. Therefore, the ordered structure of P-14 should be assigned as a hexatic columnar nematic (Φ_{HN}) phase (the Φ_{HN} phase should be between the Φ_N phase and the Φ_H phase).[53] In the case of P-11, Figure 8b shows a ring pattern at $2\theta = 5.7°$ (*d* spacing of 1.56 nm), which exhibits an isotropic intensity distribution based on the azimuthal scan (see Figure 8d). Therefore, the LC phase in P-11 should be a Φ_N phase.[53]

Furthermore, in Figure 7c,d, the intensity profiles obtained from the meridian direction (the chain axis) must be mainly attributed to the short-range ordered structure along the chain axis. In the helical conformation of isotactic vinyl polymers with large pendent groups, one repeating unit usually possesses a projection on its helical axis with a length around 0.20−0.23 nm.[54] In the Φ_H phase of poly[di(4-heptyl) vinylterephthalate] (PDHVT), the PDHVT possessed a short-range ordered periodicity of 0.415 nm along the column direction, which was attributed to the average distance between every two repeating units along the chain axis.[43] In this series of PMPCS samples, we speculate that the *d*

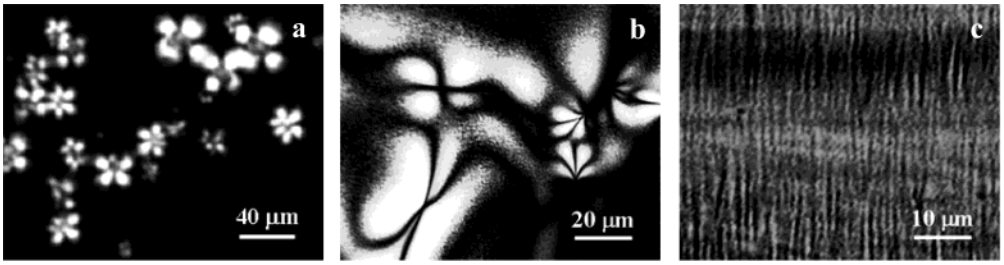

Figure 9. Two PLM images of P-14 (a) and P-11 (b) taken at 180 °C and a uniaxially sheared PLM morphology of P-14 at 200 °C (c).

spacing of nearly 0.43 nm on the meridian scattering also represents the projection of two repeating units along the chain axis. Therefore, in the case of P-14, the dimension of the *c*-axis should be 0.426 nm (see Figure 7a,c). If we use the hexagonal lattice with the dimensions of $a = b = 1.67$ nm and $c = 0.426$ nm to calculate the density (ρ) of P-14 (with two repeating units), it is 1.30 g/cm^3, while the measured ρ is 1.28 g/cm^3, which fits well with the calculated data.

The Φ_{HN} and Φ_N phase assignments can be further supported by our PLM observations. For the low M_n[a] PMPCS samples, no birefringence was observed under PLM in the temperature region studied irrespective of any thermal history (including heating, cooling, and isothermal conditions). For the samples with the high and intermediate M_n[a] values, the as-cast films did not show birefringence. However, the birefringent textures appeared during the first heating after the samples reached the temperatures at which the reflection peaks start to develop in the 1D WAXD experiments. The PLM images are presented in parts a and b of Figure 9 for the P-14 and P-11 samples, respectively, at 180 °C without mechanical shearing. Figure 9a exhibits the star-shaped textures for the P-14, which has been reported to be the characteristic feature of a columnar phase,[31,55] and in this case, it should be Φ_{HN} phase. In the P-11, a schlieren texture containing two and four brushes is evidenced in Figure 9b, implying a nematic LC structure. This LC texture of the P-11 is associated with the Φ_N phase. Both the textures of the Φ_{HN} and Φ_N phases are attributed to the anisotropic arrangements of the cylinders. The LC textures of the P-14 and P-11 remain permanently after the first heating. During the cooling to below their respective T_g values, the birefringent intensities of the samples decrease, corresponding to the reflection peak intensity decrease in the 1D WAXD patterns upon cooling.

Both the Φ_{HN} and Φ_N phases in the PMPCS samples also exhibit banded textures after mechanical shearing at high temperatures (e.g., at 200 °C) as shown in Figure 9c using the P-14 sample as an example. Since the viscosity of the samples is high, the banded textures developed slowly (over 4 h) by annealing at the shearing temperature after the external force was partially released, indicating that the relaxation of this PMPCS LC cylinder fluid was slow.

One may ask how do the PMPCS molecules form cylinders and pack into the columnar phases? We expect that each cylinder is formed by single PMPCS chain molecule.[56] Recently, structural formation in a series of polystyrene-*block*-PMPCS (PS-*b*-PMPCS) diblock copolymers was reported.[57] It was found that the PS and PMPCS blocks are microphase-separated, and the PMPCS blocks form the Φ_N phase in a similar M_n[a] range. The mesogenic groups in the PMPCS blocks

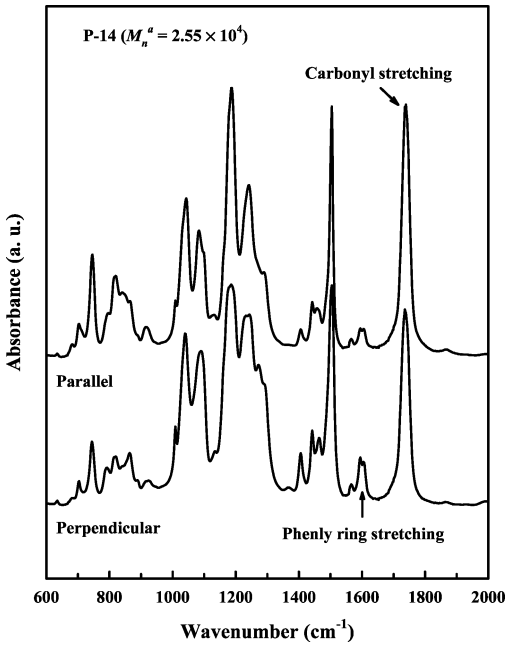

Figure 10. Polarized FT-IR spectra of oriented P-14 with 0° (parallel) and 90° (perpendicular) rotating polarized angles with respect to the shear direction. The shear direction corresponds to the meridian direction in 2D WAXD pattern in Figure 7a.

construct cylinders, which are tilted ∼52° away from the cylinder long axis.[57] On the basis of our low-angle WAXD results, the cylinder diameter is 1.67 nm for the Φ_{HN} phase in P-14, and the mesogen length is calculated to be ∼2 nm. Therefore, the mesogenic groups in the side chains tilt ∼57° away from the cylinder long axis. In the case of P-11, if we use the *d* spacing of 1.56 nm, which is the average distance between the polymer chains, to be the estimated diameter of the P-11 cylinders, a tilting angle of ∼51° is obtained for the Φ_N phase.

To gather evidence to support the idea of tilted mesogenic groups in the cylinders, we utilized polarized FT-IR experiments. Figure 10 is the spectra at 160 °C obtained in a mechanically sheared P-14 sample with the polarizing angle parallel (0°) and perpendicular (90°) to the shear direction (the meridian direction in the 2D WAXD patterns of Figure 7a). Two absorption bands at 1595 and 1605 cm^{-1} are associated with the phenyl ring stretching vibrations along the long axis of the mesogenic groups, and their intensities increase when rotating the polarizing angle from 0° to 90°. The dichroic ratios ($A_{//}/A_{\perp}$) of these two bands are 0.46 and 0.5, respectively. On the other hand, for the carbonyl stretching at 1736 cm^{-1}, which is preferentially perpendicular to the long axis of the mesogen group, the dichroic ratio is 1.1. Therefore, the mesogens tend to

be tilted away from the shear direction. We speculate that the backbones of the PMPCS molecules adopt somewhat extended conformations to generate an overall cylinder-like shape with the mesogens. The detailed chain conformation is still in an early stage of simulation.

Phase Predictions of Molecular Weight Dependence. The evolution of the ordered structures with increasing the M_n^a in this series of PMPCS samples can be explained using Flory's prediction based of his lattice model.[58] When only geometric factors are considered, a lower limit of the aspect ratio (the ratio between the length and diameter of cylinders) that is required to form a stable anisotropic phase is estimated to be 5.44. For a PMPCS cylinder with a diameter of 1.67 nm in P-14, the cylinder's long axis length should be ~9 nm at a minimum when the columnar LC phase becomes stable. This corresponds to a degree of polymerization of 42 (DP = 2 × 9/0.43), and the critical MW to generate the stable Φ_{HN} phase is thus 1.70 × 10^4 g/mol. In this study, we found that the critical M_n^a for the stable Φ_{HN} phase is approximately 1.6 × 10^4 g/mol. For the Φ_N phase, we do not exactly know the cylinder diameter on the basis of the WAXD results. If we use 1.56 nm as a rough estimation of the diameter for P-11 at room temperature, the calculated critical MW to generate the stable Φ_N phase is 1.57 × 10^4 g/mol (DP = 39) compared with experimental value of M_n^a = 1.0 × 10^4 g/mol. These differences between the M_n^as and calculated MWs may be due to that the M_n^a values of the PMPCS are underestimated by GPC calibrated using the PS standards and/or other interactions between cylinders in addition to the geometric factors.

Figure 11a depicts a set of 1D WAXD powder patterns in the low 2θ angle region for this series of PMPCS samples with various M_n^as obtained at 200 °C. The *d* spacings measured from Figure 11a are shown in Figure 11b as a function of M_n^a. For the PMPCS samples with M_n^a > 1.6 × 10^4 g/mol, the *d* spacing of the strong reflection peak is at approximately 1.48 nm representing the Φ_{HN} phase, and the relatively broad reflection is located at approximately 1.58 nm representing the Φ_N phase (see the dashed curves in Figure 11a). Therefore, in the high M_n^a PMPCS samples, the Φ_{HN} phase is developed from the Φ_N phase, and a small fraction of the Φ_N phase still exists in the sample. On the other hand, in the region of 1.0 × 10^4 g/mol ≤ M_n^a ≤ 1.6 × 10^4 g/mol, the *d* spacing of the amorphous halo is at 1.70 nm, and it coexists with the broad reflection with *d* spacing of 1.58 nm, indicating that the Φ_N phase is developed from the amorphous phase. In the low MW region of M_n^a < 1.02 × 10^4 g/mol, only the amorphous state exists.

Conclusion

In summary, combining 1D and 2D WAXD results with PLM and DSC observations, the M_n^a-dependent phase behavior in the series of PMPCS samples has been investigated. When the M_n^a < 1.0 × 10^4 g/mol, only the amorphous state can be observed despite the mesogenic nature of the side chains in these PMPCS. When 1.0 × 10^4 g/mol < M_n^a < 1.6 × 10^4 g/mol, the Φ_N phase forms. Further increasing the M_n^a to exceed 1.6 × 10^4 g/mol, the Φ_{HN} phases can develop. In the columnar LC phases, the PMPCS backbones and the laterally attached mesogenic groups cooperate together to construct cylinders as the building blocks, wherein the mesogenic side groups are found to be preferentially tilted with respect to the backbones (~51°−57°). Since the PMPCS molecules behave as rodlike chains, only in the sufficiently high M_n^a samples do the cylinders possess large enough aspect ratios to stabilize the columnar LC phases. This is the origin for the MW dependence of the LC behavior in this series of PMPCS samples. Assuming a aspect ratio of 5.44 as the lower limit in stabilizing the LC phase based on Flory's estimation, the critical cylinder lengths in the Φ_{HN} and Φ_N phases in this series of PMPCS samples should be approximately 8−9 nm, which corresponds to the DP ~ 39−42 and thus a MW of 1.57 × 10^4 g/mol (compared with the experimental observation of 1.0 × 10^4 g/mol) for the Φ_N phase and a MW of 1.70 × 10^4 g/mol (compared with the experimental observation of 1.6 × 10^4 g/mol) for the Φ_{HN} phase.

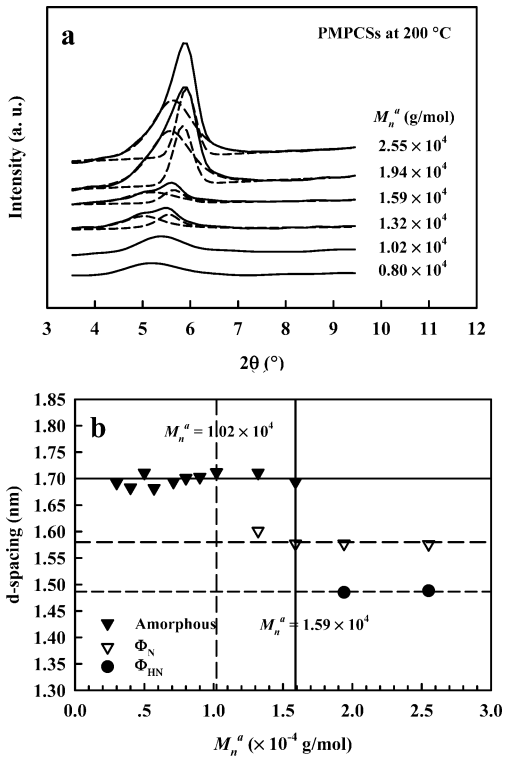

Figure 11. (a) Set of the WAXS powder patterns at 200 °C for PMPCSs with different M_n^a values. The dashed curves indicate the results of peak separations. (b) The *d* spacing measured from (a) as a function of the M_n^a. The *d* spacings of approximately 1.70, 1.58, and 1.48 nm correspond to the amorphous, the Φ_N, and the Φ_{HN} phases at 200 °C.

Acknowledgment. The financial support from the National Natural Science Foundation of China (Grants 20134010 and 20025414) is gratefully appreciated. S.Z.D.C. acknowledges his support from the US National Science Foundation (DMR-0203994).

References and Notes

(1) Donald, A. M.; Windle, A. H. *Liquid Crystalline Polymers*; Cambridge University Press: Cambridge, 1992.
(2) McArdle, C. B. *Side-Chain Liquid Crystal Polymer*; Blackie: Glasgow, 1989.
(3) Finkelmann, H.; Happ, M.; Portugall, M.; Ringsdorf, H. *Macromol. Chem.* **1978**, *179*, 2541.
(4) Hessel, F.; Finkelmann, H. *Polym. Bull. (Berlin)* **1985**, *14*, 375.
(5) Zhou, Q. F.; Li, H. M.; Feng, X. D. *Macromolecules* **1987**, *20*, 233.
(6) Zhou, Q. F.; Zhu, X. L.; Wen, Z. Q. *Macromolecules* **1989**, *22*, 491.

(7) Zhou, Q. F.; Wan, X. H.; Zhu, X. L.; Zhang, F.; Feng, X. D. *Mol. Cryst. Liq. Cryst.* **1993**, *231*, 107.
(8) Zhou, Q. F.; Wan, X. H.; Zhu, X. L.; Zhang, D.; Feng, X. D. In *Liquid Crystalline Polymer Systems−Technological Advances*; Isayev, A. I., Kyu, T., Cheng, S. Z. D., Eds.; ACS Symposium Book Series 632; American Chemical Society: Washington, DC, 1996; pp 344−357.
(9) Zhang, D.; Zhou, Q. F.; Ma, Y. G.; Wan, X. H.; Feng, X. D. *Polym. Adv. Technol.* **1997**, *8*, 227.
(10) Zhang, D.; Liu, Y. X.; Wan, X. H.; Zhou, Q. F. *Macromolecules* **1999**, *32*, 5183.
(11) Tu, Y. F.; Wan, X. H.; Zhang, D.; Zhou, Q. F.; Wu, C. *J. Am. Chem. Soc.* **2000**, *122*, 10201.
(12) Tu, Y. F.; Wan, X. H.; Zhang, H. L.; Fan, X. H.; Chen, X. F.; Zhou, Q. F.; Chau, K. *Macromolecules* **2003**, *36*, 6565.
(13) Zhang, H.; Yu, Z.; Wan, X.; Zhou, Q.; Woo, E. M. *Polymer* **2002**, *43*, 2357.
(14) Yu, Z. N.; Wan, X. H.; Zhang, H. L.; Chen, X. F.; Zhou, Q. F. *Chem. Commun.* **2003**, 974.
(15) Yu, Z. N.; Tu, H. L.; Wan, X. H.; Chen, X. F.; Zhou, Q. F. *J. Polym. Sci., Part A: Polym. Chem.* **2003**, *41*, 1454.
(16) Xu, G. Z.; Wu, W.; Shen, D. Y.; Hou, J. N.; Zhang, S. F.; Xu, M.; Zhou, Q. F. *Polymer* **1993**, *34*, 1818.
(17) Wan, X. H.; Zhang, F.; Wu, P.; Zhang, D.; Feng, X. D.; Zhou, Q. F. *Macromol. Symp.* **1995**, *96*, 207.
(18) Hardouin, F.; Mery, S.; Achard, M. F.; Noirez, L.; Keller, P. *J. Phys. II* **1991**, *1*, 511, and Erratum, 871.
(19) Hardouin, F.; Leroux, N.; Mery, S.; Noirez, L. *J. Phys. II* **1992**, *2*, 271.
(20) Leroux, N.; Keller, P.; Achard, M. F.; Noirez, L.; Hardouin, F. *J. Phys. II* **1993**, *3*, 1289.
(21) Arehart, S. V.; Pugh, C. *J. Am. Chem. Soc.* **1997**, *119*, 3027.
(22) Pugh, C.; Shao, J.; Ge. J. J.; Cheng, S. Z. D. *Macromolecules* **1998**, *31*, 1779.
(23) Pugh, C.; Bae, J.-Y.; Dharia, J.; Ge, J. J.; Cheng, S. Z. D. *Macromolecules* **1998**, *31*, 5188.
(24) Kim, G.-H.; Pugh, C.; Cheng, S. Z. D. *Macromolecules* **2000**, *33*, 8983.
(25) Small, A. C.; Pugh, C. *Macromolecules* **2002**, *35*, 2105.
(26) Pragliola, S.; Ober, C. K.; Mather, P. T.; Jeon, H. G. *Macromol. Chem. Phys.* **1999**, *200*, 2338.
(27) Lecommandoux, S.; Noirez, L.; Achard, M. F.; Hardouin, F. *Macromolecules* **2000**, *33*, 67.
(28) Shen, Z. H. Ph.D. Dissertation, Department of Polymer Science, University of Akron, 2001.
(29) Kreuder, W.; Ringsdorf, H. *Makromol. Chem., Rapid Commun.* **1983**, *4*, 807.
(30) Kreuder, W.; Ringsdorf, H.; Tschirner, P. *Makromol. Chem., Rapid Commun.* **1985**, *6*, 367.
(31) Wenz, G. *Makromol. Chem., Rapid Commun.* **1985**, *6*, 577.
(32) Herrmann-Schonherr, O.; Wendorff, J. H.; Kreuder, W.; Ringsdorf, H. *Makromol. Chem., Rapid Commun.* **1986**, *7*, 97.
(33) Huser, B.; Spiess, H. *Makromol. Chem., Rapid Commun.* **1988**, *9*, 337.
(34) Ringsdorf, H.; Wustefeld, R.; Zerta, E.; Ebert, M.; Wendorff, J. H. *Angew. Chem., Int. Ed. Engl.* **1989**, *28*, 914.
(35) Weck, M.; Mohr, B.; Maughon, B. R.; Grubbs, R. H. *Macromolecules* **1997**, *30*, 6430.
(36) Stewart, D.; McHattie, G. S.; Imrie, C. T. *J. Mater. Chem.* **1998**, *8*, 47.
(37) Kouwer, P. H. J.; Jager, W. F.; Mijs, W. J.; Picken, S. J. *Macromolecules* **2000**, *33*, 4336.
(38) Kouwer, P. H. J.; Jager, W. F.; Mijs, W. J.; Picken, S. J. *Macromolecules* **2002**, *35*, 4322.
(39) Zheng, R. Q.; Chen, E. Q.; Cheng, S. Z. D.; Xie, F. C.; Yan, D. H.; He, T. B.; Percec, V.; Chu, P.; Ungar, G. *Macromolecules* **1999**, *32*, 3574.
(40) Zheng, R. Q.; Chen, E. Q.; Cheng, S. Z. D.; Xie, F. C.; Yan, D. H.; He, T. B.; Percec, V.; Chu, P.; Ungar, G. *Macromolecules* **1999**, *32*, 6981.
(41) Zheng, R. Q.; Chen, E. Q.; Cheng, S. Z. D.; Xie, F. C.; Yan, D. H.; He, T. B.; Percec, V.; Chu, P.; Ungar, G. *Macromolecules* **2000**, *33*, 5159.
(42) Zhang, D.; Liu, Y. X.; Wan, X. H.; Zhou, Q. F. *Macromolecules* **1999**, *32*, 4494.
(43) Tu, H. L.; Wan, X. H.; Liu, Y. X.; Chen, X. F.; Zhang, D.; Zhou, Q. F.; Shen, Z. H.; Ge, J. J.; Jin, S.; Cheng, S. Z. D. *Macromolecules* **2000**, *33*, 6315.
(44) Yin, X. Y.; Chen, E. Q.; Wan, X. H.; Zhou, Q. F. *Chin. J. Polym. Sci.* **2003**, *21*, 9.
(45) Yin, X. Y.; Ye, C.; Ma, X.; Chen, E. Q.; Qi, X. Y.; Duan, X. F.; Wan, X. H.; Cheng, S. Z. D.; Zhou, Q. F. *J. Am. Chem. Soc.* **2003**, *125*, 6854.
(46) Liu, Z.; Zhu, L.; Zhou, W.; Cheng, S. Z. D.; Percec, V.; Ungar, G. *Macromolecules* **2002**, *35*, 9426.
(47) Percec, V.; Heck, J.; Tomazos, D.; Falkenberg, F.; Blackwell, H.; Ungar, G. *J. Chem. Soc., Perkin Trans. 1* **1993**, 2799.
(48) Percec, V.; Ahn, C. H.; Barboiu, B. *J. Am. Chem. Soc.* **1997**, *119*, 12978.
(49) Percec, V.; Ahn, C. H.; Ungar, G.; Yeardley, D. J. P.; Moller, M.; Sheiko, S. S. *Nature (London)* **1998**, *391*, 161.
(50) Forster, S.; Neubert, I.; Schluter, A. D.; Linder, P. *Macromolecules* **1999**, *32*, 4043.
(51) Liu, Y. X.; Zhang, D.; Wan, X. H.; Zhou, Q. F. *Chin. J. Polym. Sci.* **1998**, *16*, 283.
(52) Wunderlich, B. *Thermal Analysis*; Academic Press: New York, 1990.
(53) de Genes, P. G.; Prost, J. *The Physics of Liquid Crystals*; Oxford: New York, 1993.
(54) Wunderlich, B. *Macromolecular Physics*; Academic Press: New York, 1973; Vol. I.
(55) Gray, G. W.; Goodby, J. W. *Smectic Liquid Crystals−Textures and Structure*; Leonhard Hill: Glasgow, 1984; Appendix plates No. 123, 124.
(56) We have also studied the phase behaviors of the PMPCS monomer. It was found that the monomers are in a crystalline state below 110 °C. Above this temperature, both the WAXD and PLM experiments revealed that the monomers exhibited a nematic LC phase formed by the mesogenic groups. The monomers at this temperature, however, also underwent a thermal polymerization. With increasing the degree of polymerization to form oligomers, this nematic LC phase gradually disappeared and enters the amorphous phase. At the later stage where the large degree of polymerization led to the high M_n[a] PMPCS, the resulting polymers exhibited the low 2θ angle diffraction in WAXD experiments, which was associated with the columnar phase formation. This nematic to amorphous to columnar phase evolution with increasing the M_n[a] of PMPCS clearly indicated that the ordered phase structures observed in the PMPCS samples were attributed to the building blocks of cylinders.
(57) Li, C. Y.; Tenneti, K. K.; Zhang, D.; Zhang, H.; Wan X.; Chen, E. Q.; Zhou, Q. F.; Carlos, A.-O.; Igos, S.; Hsiao, B. S. *Macromolecules* **2004**, *37*, 2854.
(58) Flory, P. J. *Proc. R. Soc. London* **1956**, *A234*, 73.

MA049195B